BIO-SYNTHESIS AND BIOLOGICAL ACTIVITIES OF $CoFe_2O_4$/Ag NANOPARTICLES USING MALE CARICA PAPAYA L. LEAF AND FLOWER EXTRACT

Đến tòa soạn 05-01-2023

Thao Truong Thi, Duangphachanh Itphavanh, Giang Ngo Thi, Tham Diep Thi Hong
TNU-University of Sciences, Thai Nguyen University, Tan Thinh ward, Thai Nguyen City
*Email: thao.tt@tnus.edu.vn

TÓM TẮT

TỔNG HỢP SINH HỌC VÀ KHẢO SÁT HOẠT TÍNH SINH HỌC CỦA PHỨC HỆ NANO $CoFe_2O_4$/Ag SỬ DỤNG DỊCH CHIẾT LÁ VÀ HOA ĐU ĐỦ ĐỰC

Nghiên cứu này trình bày kết quả tổng hợp vật liệu nano cobalt ferrite $CoFe_2O_4$/Ag sử dụng dịch chiết lá và hoa đu đủ đực bằng phương pháp đồng kết tủa kết hợp với quá trình oxi hóa quang hóa Ag^+ bằng đèn UV ở nhiệt độ thường (Ký hiệu là CAx.CP). Cấu trúc, hình thái vật liệu, từ tính của các vật liệu tổng hợp được được xác định bằng các phương pháp nhiễu xạ tia X (XRD), phổ hồng ngoại (FTIR), phổ tán xạ năng lượng (EDX), từ kế mẫu rung (VSM), chụp ảnh hiển vi điện tử quét SEM và ảnh hiển vi điện tử truyền qua TEM. Các vật liệu sạch, đưa được dịch chiết và Ag với tỷ lệ mong muốn lên CFO. Các mẫu CAx.NPs được đánh giá khả năng kháng các vi khuẩn gram âm (P. aeruginosa, E.coli) và vi khuẩn gram dương (S. aureus) theo phương pháp khuếch tán đĩa thạch. Khả năng kháng khuẩn tốt nhất là vật liệu CA20.CP, đường kính vòng kháng khuẩn S. aureus, P. aeruginosa and E.coli tại nồng độ 150 µg/mL tương ứng lần lượt là 34, 32 and 29 mm. Đây cũng là vật liệu có kích thước nhỏ nhất và phân tán đồng đều nhất trong các vật liệu tổng hợp được. Khả năng gây độc tế bào ung thư biểu mô KB của CA20.CP tốt hơn CFO với IC_{50} đạt 76.32 µg/mL. Các kết quả này cho thấy tiềm năng ứng dụng cao của vật liệu tổng hợp được.

Từ khóa: *tổng hợp sinh học, CFO/Ag, đu đủ đực, kháng khuẩn, chống ung thư*

1. INTRODUCTION

Cobalt ferrite $CoFe_2O_4$ (CFO) is a ferromagnetic material with a cubic inverse spinel structure that has the potential to be widely applied in various interdisciplinary fields ranging from information storage, electronic devices, electromagnetic interference suppressors, electromagnetic wave absorbers, sensors, catalytic to the environment, medical [1], [2]. CFO has excellent magnetic and electrical properties, maximum coercive field (Hc), chemical stability and mechanical hardness. These specific properties make the CFO a potential candidate for biomedical applications, such as magnetic resonance imaging, drug delivery, antibacterial, anticancer, and hyperthermia [3]. The use of CFO NPs as an antimicrobial agent against pathogenic and anticancer agents against cancer cell lines has been a new and intriguing field.

Many different methods were reported in the literature for the synthesis of CFO, such as solid-state reaction method, ball milling method, sol-gel, combustion, microemulsion, co-precipitation, hydrothermal method, etc. [4]. The biosynthetic method using plant extract or microorganisms, enzymes, etc, has been growing strong recently. Bio-synthesis has been suggested as the possible eco-friendly, relatively straightforward. With nanomaterial for medical, the biosynthetic route enhances benignity and effectiveness because plant extracts (special folk medicinal plants) contain many promising

bioactive compounds. Furthermore, plant extracts can participate in the synthesis process as a surfactant due to their rich composition of natural organic compounds (polyphenols, terpenoids, flavonoids, monoterpenes, tri-terpenes, etc), provides high-yield nanomaterials with the well crystalline structure and desirable properties.

Many nano-material were synthesized using plant extract, such as ZnO, Ag, Au, CuO, ….[5]. There are some studies focussing on biosynthesis of CFO, such as extract of *Crataegus microphylla* fruit [2], aloe vera [6], okra [7], olive leaf [8], garlic and tulsi seed [9], hibiscus *rosa sinesis* leaf [10] and sesame seed [11]. However, there have been no published studies on the biosynthesis of CFO NPs by extract of male *Carica papaya* L. leaf or flower.

Carica papaya L. is one of the ubiquitous and vital fruits in tropical and subtropical regions. The whole parts, including fruit, root, bark, peel, seed and pulp of papaya are known to apply as a medicinal therapy. They are a rich source of three powerful antioxidant vitamin C, vitamin A and vitamin E, and also consist of minerals, such as magnesium and potassium, fiber and critical phytochemicals. These mentioned substances have been reported to be an antioxidant, antibacterial, anticancer activity, anti-fertility agent, anti-inflammatory, antiulcer, antidiabetic, protective liver, improving the cardiovascular system, protecting against heart diseases, heart attacks, strokes and preventing colon cancer, treating causes of trauma, allergies and sports injuries [12]–[14]. *Carica papaya* L. was used for preparing some nano-materials such as copper oxide [15], silver [16], iron oxide [17] and zinc oxide [18].

Besides, some researchers have conducted chemically synthesized and biosynthesized CFO or CFO/Ag on antibacterial and anti-cancer drug delivery [9], [10], [19], [20]; however, very few results focusing on the cytotoxic cancer cell line have been published so far.

In this study, CFO/Ag nano-material was synthesized via the bio-synthesis using male *Carica papaya* L. leaf and flower extract (CAx.CP). A three-step fabrication process was applied to improve antibacterial activity against Gram-negative (*P. aeruginosa* and *E. coli*) and Gram-positive (*S. aureus*) bacterial and anticancer activity against KB cancer cell.

2. EXPERIMENT

2.1. Materials

All chemicals were of analytical grade and used without further purification, including silver nitrate ($AgNO_3$), cobalt nitrate ($Co(NO_3)_2{\cdot}6H_2O$), iron nitrate ($Fe(NO_3)_3{\cdot}9H_2O$ and sodium hydroxide (NaOH) as a mineralizer. Dimethyl sulfoxide (DMSO) was used as a solvent for antibacterial testing. *Carica papaya* L. (*CP*) leaves and flowers were collected in Thai Nguyen province, Vietnam.

2.2. Preparation and characterization of CAx.CP NPs

Preparation of Carica papaya L. leaf and flower extract: Fresh *Carica papaya* L. leaf and flower were washed several times using distilled water, dried in an oven at 50^{o}C for 24 h, then chopped into small pieces and soaked in 100 mL of Milli-Q water in an Erlenmeyer flask and warmed at 50^{0}C for 10 min. 10 g of *Carica papaya* L. leaf and flower was ultrasound extracted by 100 mL of ethanol for 1 hour at 60^{o}C. The extract was cooled, filtered, and stored at 4°C for further experiments, and denoted CP extract.

Bio-synthesis of nanomaterial: The mixture of 0.005 mole $Co(NO_3)_2$ and 0.01 mole $Fe(NO_3)_3$ was completely dissolved in 30 mL distilled water (DW). Then, 50 mL of 1M NaOH aqueous solution was added dropwise into the above salt solution, and then it was stirred at room temperature for 90 min to get a suspension system. Then 5 ml of CP extract was added drop by drop into the suspension system in stirring for 60 min. Finally, 20 ml solution of x mole $AgNO_3$ (where x = 1, 5, 10, 20 % the mole of Co^{2+}) was added dropwise into the above system under continuous stirring and UV illumination (wavelength of 254 nm) for 60 min. The suspension was centrifuged to neutralise by washing it with ethanol and DW. The precipitate was dried at 110 °C for 24 h, then grounded and stored for further experiments. Samples were designed as CA1.CP; CA5.CP; CA10.CP and CA20.CP. The same procedure without adding $AgNO_3$ solution gives the product abbreviated as CFO.CP, while the procedure without adding CP extract and $AgNO_3$ solution formed the product abbreviated as CFO.

Characterization: The samples' X-ray diffraction (XRD) patterns were employed by Bruker AXS XRD equipment at 45 kV and 40 mA, room temperature. The FTIR spectra were done by FT/IR-4600 spectrophotometer in the range of

4000-400 cm^{-1} using the KBr pellet technique. The elemental analysis using dispersive energy X-ray (EDX, EDAX Genesis). The size and morphology were analyzed using scanning electron microscopy (SEM) (Hitachi S-4800) and transmission electron microscopy (TEM). Hysteresis loops were recorded at room temperature to the highest field of 11 kOe, employing a DMS 880 Vibrational Sample Magnetometer.

2.3. Assays for biological activities

2.3.1. Antibacterial activity

The prepared samples were dispersed in DMSO and evaluated the antibacterial activity by the agar diffusion method [21] against Gram-negative (*P. aeruginosa* and *E. coli*) and Gram-positive (*S. aureus*) bacterial. Petri plates containing Muller Hinton Agar Medium were seeded with three bacterial strains. Wells, which had a diameter of approximately 8 mm, were bored using a good cutter, and different concentrations of samples were added. It was then incubated at 37°C for 24 h and the zone of inhibition was measured in millimeters (mm). A 2% DMSO solution was a blank solution.

2.3.2. Cytotoxic activity against KB cancer cell line

The anticancer activity of CFO and CA20.CP against KB cancer cells was evaluated using the MTT method at concentrations of 2, 8, 32, 64 and 128 µg/mL. Control cell was treated with the amount of DMSO equal to the one used to treat cells. The extent of cell proliferation was indirectly determined by measuring optical density at 570 nm on a multi-spectrometer (Multiskan Sky, Thermo Fisher). The IC_{50} value was calculated based on the OD absorbance using the specialized software GraphPad Prism 5.0 according to the manufacturer's instructions.

3. RESULTS AND DISCUSSION

3.1. Characterization

Characterization of synthesized materials is shown in Fig 1 and Fig.2.

From Fig. 1a, the CFO and CFO/Ag samples can be assigned to the inverse spinel structure according to the standard XRD patterns (JCPDS Patterns No. 21-1272). The peaks with 2θ values of 30.1°, 35.5°, 43.1°, 53.5°, 57.1° and 62.7° corresponded to the crystal planes (220), (311), (400), (422), (511), and (440) of crystalline $CoFe_2O_4$, respectively. The crystallite size (D) was calculated using the Scherrer equation:

$$D = 0.89\lambda/\beta.\cos\theta$$

Where λ is the wavelength of Cu Ka (0.15406 nm), β is the full width at half maximum, and θ is the diffraction angle [22].

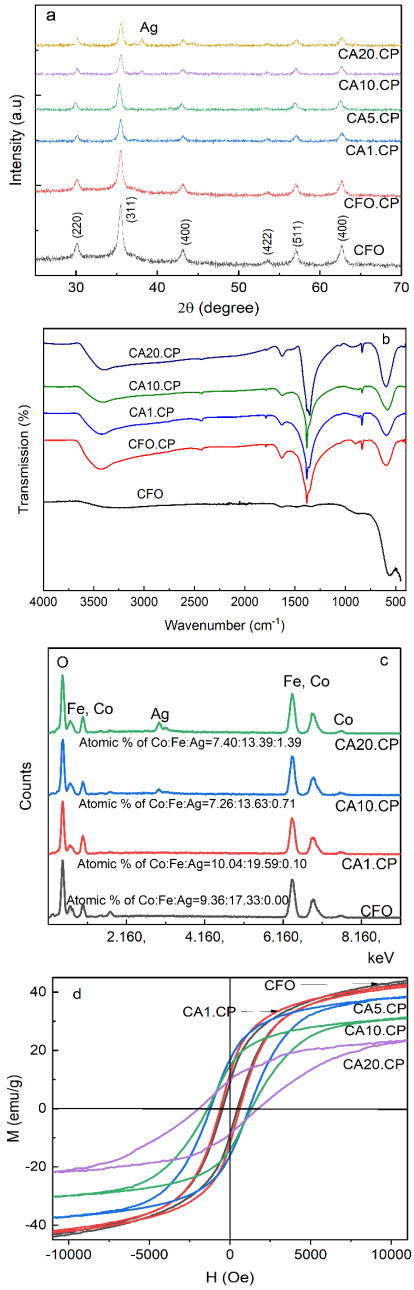

Fig.1. a) X-ray diffraction pattern, b) IR spectrum, c) EDX spectrum and d) Hysteresis loops of CAx.CP samples

The average crystallite size calculated from the (311) peak of the crystal plane using Scherrer's equation were 29.3, 28.8, 37.3, 33.8, 31.0 and 29.7 nm for CFO, CFO.CP, CA1.CP, CA5.CP, CA10.CP and CA20.CP, respectively.

No peaks belonging to any other phase were identified. The diffraction peak position of

(311) crystal plane of CFO.CP coincided with CFO, indicating that the catching of CP extract on CFO did not affect to CFO crystal structure. When Ag attacked to CFO, on the CA1.CP spectra, the peaks with Ag species could not be observed, possibly due to the low doping content of Ag in the sample. In addition, the position of diffraction peaks shifted toward a slight angle with the increase of Ag amount, the peak intensity of Ag increased, and the diffraction peak of CAx.CP spectrum slightly altered toward the higher angle compared with CFO. This result indicated that a small amount of Ag was incorporated into the CFO structure, substituting sites. It increased of crystal size of CA1.CP and CA5.CP compared with CFO, but as x increased, the crystal size decreased. It might be speculated that Ag crystallized into the crevices of the CFO matrix, leading to better particle distribution. Thus, biosynthesized CFO/Ag NPs were successfully prepared through a three-step fabrication process.

The FTIR spectra of CAx.CP NPs are shown in Fig. 1b. The FTIR spectrum of CFO merely consists of a characteristic peak in the range of 400–700 cm^{-1} are related to the metal–O bond and a broad absorption peak at around 3300 cm^{-1} belonged to the stretching vibration of the moisture O-H bond [2]. In the CAx.CP spectra, the characteristic peak of metal-O in the range of 400-700 cm^{-1} shifted toward to higher wavenumber and spectrum appeared some new adsorption peaks: 835 cm^{-1} attributed to the presence of C-C bond in alkane group [23], 1354 cm^{-1},1381 cm^{-1}, 1638 cm^{-1}, 1788 cm^{-1} were associated with the C–N, C–C, –C=C–, and –C=O stretching vibrations of aromatic amines, alkenes, aromatics and carbonyl [24], [25], 2434 cm^{-1} belonged to C≡C triple bonds and the broad absorption peaks at around 3300 cm^{-1} shifted to about 3435 cm^{-1} can be due to C-H, O-H stretch and the interaction between CP extract and CFO NPs [26]. These results suggest that the CP extract was captured on the CFO structure. The result of the FTIR of this study was consistent with the FTIR spectrum of CFO NPs synthesized from various plant extracts [2], [6], [7].

In Fig.1c, EDX elemental analysis of some prepared samples proved the existence of Fe, Co and O elements in CFO spectra and the co-existence of Co, Fe, Ag and O elements in CAx.CP; atomic % of Ag in samples was approximately the desired value in sample preparation.

Magnetization versus applied magnetic field (M–H) curves of the samples were measured and shown in Fig.1d. The value of the saturation magnetization (Ms) for CFO was about 44.1 emu/g. Moreover, as the quantity of Ag attacked CFO increased, the Ms decreased, but the values of coercivity (*Hc*) increased. This result was in agreement with Li's study, which reported that by doping a small amount of Cr into CFO, Hc also increased due to Cr substituted CFO structure leading to the migration of Co ion from octahedral to tetrahedral sites [27].

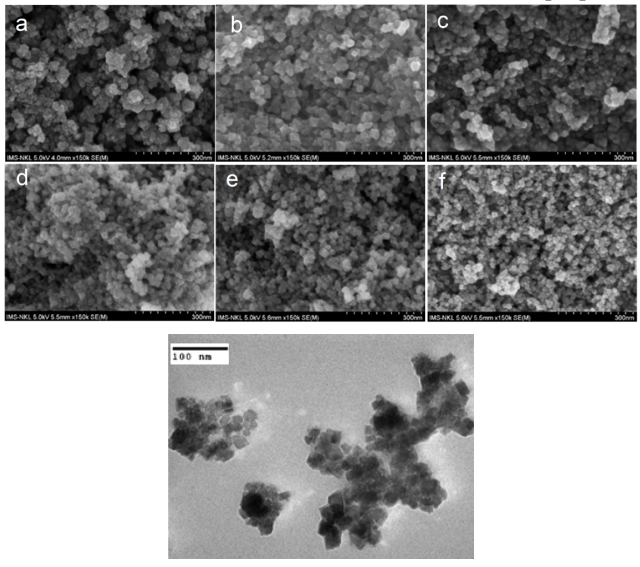

Fig. 2. SEM images of a) CFO, b) CFO.CP, c) CA1.CP, d) CA5.CP, e) CA10.CP, f) CA20.CP and TEM of CA20.CP

The SEM image of pure CFO (Fig.2a) shows that the particles are smaller than CFO.CP, but there is the phenomenon of agglomeration into heterogeneous granules. The SEM image of CFO.CP (Fig.2b) shows the particles with high uniformity in shape and size. It indicates that CP extract effectively acted as a surfactant, preventing the particles from agglomeration and dispersing evenly. In Ag-attacked CFO samples, as Ag content increased (Fig.2c to Fig. 2f), the particle size decreased, and the size of CA20.CP was the smallest and the most uniform distribution. This result may be the influence of Ag content and the form of Ag precipitates in the CFO structure lattice as analyzed by XRD spectra. The rule of resizing between CAx.CP samples were consistent with the calculation results according to the Scherrer equation, but the value was smaller.

3.2. Application of prepared samples

Antibacterial activity

Antibacterial activity of CFO/Ag NPs was carried out against *P. aeruginosa, S. aureus* and *E.coli*.

The growth inhibitory effect of organisms in the agar well diffusion method is presented in Table. 1.

Table 1 show that the antibacterial activity of CFO was somewhat intense for three types of bacterial at 250 *µg/mL* (better than in results of Gheidari [28]); CP extracts inhibited for *P. aeruginosa, S. aureus* but did not for E.coli. And the antibacterial activity CFO.CP all increased in comparison with CP extract and CFO for all bacteria. It means that the CFO-capturing CP extract increases the effectiveness of the CFO against the above bacteria. And the antibacterial activity of CAx.CP increased with the increase of Ag amount. As the analysis results above, when the Ag content in the sample increased, the particle size decreased, the homogeneity increased, the dispersion increased, and leading to an increase in the antibacterial ability. The antibacterial activity of CA20.CP also increased with the rise in the sample concentration. And the inhibition zone diameter of 150 *µg/mL* CA20.CP was the same as 250 *µg/mL CFO.CP*. It means that the Ag attacked the CFO.CP significantly increased the antibacterial effectiveness of CFO.CP. These results were consistent with other materials which were biosynthesized from a plant extract or Ag attacked [7], [20]; and the antibacterial effectiveness was higher than some other reports in which CFO-capturing plant extract and Ag NPs [9], [10]. The CA20.CP sample continued to evaluate the cytotoxic activity against the KB cancer cell line.

Table 1. The inhibition zone diameter of CAx.CP samples against P.aeruginosa, S.aureus and E.coli (d=mm)

No	Sample	Concentration	The inhibition zone diameter (mm)		
			P.aeruginosa	*S.aureus*	*E.coli*
1	*CFO*	250 (*µg/mL*)	25	28	24
2	*CFO.CP*	250 (*µg/mL*)	31	33	30
3	*CP extract*	250 *(µL/mL)*	22	25	0
4	*DMSO*	100 (%)	0	0	0
5	*CA1.CP*	100 (*µg/mL*)	18	20	20
6	*CA5.CP*		22	24	22
7	*CA10.CP*		24	27	24
8	*CA20.CP*		28	30	27
9	*CA20.CP*	25 (*µg/mL*)	15	17	10
10		50 (*µg/mL*)	20	23	19
11		100 (*µg/mL*)	27	29	25
12		150 (*µg/mL*)	34	32	30

Anticancer activity

The KB cancer cells were treated with different doses of CFO and CA20.CP (2–128 µg/mL) for 72h with Ellipticine used as the positive control (IC_{50} = 0.31 ± 0.05 µg/mL).

The results exhibited that the percentage of inhibition of the cancer cell line significantly increased from 0 to 65% and 86% with increasing concentrations of the CFO and CA20.CP samples from 2 to 128 µg/mL. IC_{50} value of CFO and CA20.CP NPs are 99.7 ± 1.68 and 76.32±2.0 µg/mL, respectively.

The CA20.CP NPs showed moderate toxicity against the KB cells growth compared with the ZnO synthesized using the aqueous leaf extract of Laurus nobilis, inhibiting the viability of human A549 lung cancer cells with IC_{50} of 80 µg/mL [23], or ZnO using *Tecoma castanifolia* leaf extract with IC_{50} of 65 µg/mL for A549 [29]. This result opens the potential to apply CFO/Ag NPs synthesized from PC extract to synthesize drugs to treat human epithelial carcinoma cells.

4. CONCLUSION

Silver-cobalt ferrite CFO/Ag NPs have been successfully bio-synthesized using male *Carica papaya* L. leaf and flower by co-precipitation method combination with Ag^+ photochemical oxidation by UV lamp at room temperature. All prepared materials are pure, nanometer size, CP extract and Ag were caught into the CFO structure. CP extract acted as an effective surfactant, proving particles' dispersion and uniformity, significantly reducing particles' agglomeration. The catching of CP extract and Ag enhances the antibacterial and anticancer activity of CFO. The best antibacterial activity against *S. aureus, P. aeruginosa* and *E.coli* is 150 µg/mL CA20.CP NPs, the zone of inhibition diameter are 34, 32 and 29 mm, respectively. The cytotoxic activity against KB cancer cell line of CA20.CP NPs increase (IC_{50}= 76.32 µg/mL) compared with CFO (99.7 µg/mL). This result opens the potential for applying CFO/Ag NPs synthesized from male *Carica papaya* L. extract to synthesize drugs for treating human epithelial carcinoma cells.

REFERENCES

[1] K. Elayakumar et al., (2019). Structural, morphological, enhanced magnetic properties and antibacterial bio-medical activity of rare earth element (REE) cerium (Ce^{3+}) doped $CoFe_2O_4$ nanoparticles. *J. Magn. Magn. Mater.*, **vol. 476**, pp. 157–165.

[2] A. Naghizadeh, S. Mohammadi-Aghdam, and S. Mortazavi-Derazkola, (2020). Novel $CoFe_2O_4$@ZnO-CeO_2 ternary nanocomposite: Sonochemical green synthesis using Crataegus microphylla extract, characterization and their application in catalytic and antibacterial activities. *Bioorg. Chem.*, **no. June**, p. 104194.

[3] L. Horev-Azaria et al., (2013). Predictive Toxicology of cobalt ferrite nanoparticles: Comparative in-vitro study of different cellular models using methods of knowledge discovery from data. *Part. Fibre Toxicol.*, **vol. 10**, no.1, pp. 1–17.

[4] F. Sharifianjazi et al., (2020). Magnetic $CoFe_2O_4$ nanoparticles doped with metal ions: A review. *Ceram. Int.*, **vol. 46**, no. 11, pp. 18391–18412.

[5] E. Sánchez-López et al., (2020). Metal-based nanoparticles as antimicrobial agents: An overview. *Nanomaterials*, **vol. 10**, no.2, pp. 1–43.

[6] A. Manikandan, R. Sridhar, S. Arul Antony, and S. Ramakrishna, (2014). A simple aloe vera plant-extracted microwave and conventional combustion synthesis: Morphological, optical, magnetic and catalytic properties of $CoFe_2O_4$ nanostructures. *J. Mol. Struct.*, **vol. 1076**, pp. 188–200.

[7] K. Kombaiah, J. J. Vijaya, L. J. Kennedy, M. Bououdina, R. J. Ramalingam, and H. A. Al-Lohedan, (2018). Okra extract-assisted green synthesis of $CoFe_2O_4$ nanoparticles and their optical, magnetic, and antimicrobial properties. *Mater. Chem. Phys.*, **vol. 204**, pp. 410–419.

[8] S. S. Banifatemi, F. Davar, B. Aghabarari, J. A. Segura, F. J. Alonso, and S. M. Ghoreishi, (2021). Green synthesis of $CoFe_2O_4$ nanoparticles using olive leaf extract and characterization of their magnetic properties. *Ceram. Int.*, **vol. 47**, no.13, pp. 19198–19204

[9] P. Mahajan, A. Sharma, B. Kaur, N. Goyal, and S. Gautam, (2019). Green synthesized (*Ocimum* sanctum and *Allium* sativum) Ag-doped cobalt ferrite nanoparticles for antibacterial application. *Vacuum*, **vol. 161**, no. July 2018, pp. 389–397.

[10] Gingasu et al., (2016). Green Synthesis Methods of $CoFe_2O_4$ and Ag-$CoFe_2O_4$ Nanoparticles Using *Hibiscus* Extracts and Their Antimicrobial Potential. *J. Nanomater.*, **vol. 2016**, p. 1-12.

[11] D. Gingasu et al., (2016). Synthesis of nanocrystalline cobalt ferrite through soft chemistry methods: A green chemistry approach using sesame seed extract. *Mater. Chem. Phys.*, **vol. 182**, pp. 219–230.

[12] A. Sharma, A. Bachheti, P. Sharma, R. K.

Bachheti, and A. Husen, (2020). Phytochemistry, pharmacological activities, nanoparticle fabrication, commercial products and waste utilization of *Carica papaya* L.: A comprehensive review. *Curr. Res. Biotechnol.*, **vol. 2,** no. September, pp. 145–160.
[13] S. Habtemariam, (2019). *The chemical and pharmacological basis of papaya (Carica papaya L.) as potential therapy for type-2 diabetes and associated diseases*. Chapter 11, Elsevier Ltd.
[14] T. Vij and Y. Prashar, (2015). A review on medicinal properties of Carica papaya Linn. *Asian Pacific J. Trop. Dis.*, **vol. 5**, no. 1, pp.1–6.
[15] R. Sankar, P. Manikandan, V. Malarvizhi, T. Fathima, K. S. Shivashangari, and V. Ravikumar, (2014). Green synthesis of colloidal copper oxide nanoparticles using *Carica papaya* and its application in photocatalytic dye degradation. *Spectrochim. Acta - Part A Mol. Biomol. Spectrosc.*, **vol. 121**, no.75, pp. 746–750.
[16] R. R. Banala, V. B. Nagati, and P. R. Karnati, (2015). Green synthesis and characterization of *Carica papaya* leaf extract coated silver nanoparticles through X-ray diffraction, electron microscopy and evaluation of bactericidal properties. *Saudi J. Biol. Sci.*, **vol. 22**, no.5, pp. 637–644.
[17] M. S. H. Bhuiyan et al., (2020). Green synthesis of iron oxide nanoparticle using *Carica papaya* leaf extract: application for photocatalytic degradation of remazol yellow RR dye and antibacterial activity. *Heliyon*, **vol. 6**, no.8, p. e04603.
[18] C. Vidya, C. Manjunatha, M. N. Chandraprabha, M. Rajshekar, and M. A. L. Antony Raj, (2017). Hazard free green synthesis of ZnO nano-photo-catalyst using *Artocarpus Heterophyllus* leaf extract for the degradation of Congo red dye in water treatment applications. *J. Environ. Chem. Eng.*, **vol. 5**, no.4, pp. 3172–3180.
[19] M. Ghanbari, F. Davar, and A. E. Shalan, (2021). Effect of *rosemary* extract on the microstructure, phase evolution, and magnetic behavior of cobalt ferrite nanoparticles and its application on anti-cancer drug delivery. *Ceram. Int.*, **vol. 47**, no.7, pp. 9409–9417.
[20] S. Gankhuyag, K. Lee, and D. S. Bae, (2018). Facile Synthesis of Efficient Antibacterial Agent as $CoFe_2O_4$/Ag Composite Material Against Both Gram-Negative Escherichia coli and Gram-Positive Bacillus subtilis Bacteria. *J. Nanosci. Nanotechnol.*, **vol. 18**, no.9, pp. 6348–6354.
[21] M. Balouiri, M. Sadiki, and S. K. Ibnsouda, (2016). Methods for in vitro evaluating antimicrobial activity: A review. *J. Pharm. Anal.*, **vol. 6**, no.2, pp. 71–79.
[22] Lê Thị Thanh Thúy, Nguyễn Hữu Lân, (2020).
Enhanced photocatalytic performance of visible light TiO_2. *Journal of Analytical Sciences*, Vietnam analytical sciences society, **Vol 25**, No 1/2020, p. 130-136.
[23] S. Vijayakumar, B. Vaseeharan, B. Malaikozhundan, and M. Shobiya, (2016). Laurus nobilis leaf extract mediated green synthesis of ZnO nanoparticles: Characterization and biomedical applications. *Biomed. Pharmacother.*, **vol. 84**, pp. 1213–1222.
[24] S. Vasantharaj et al., (2021). Enhanced photocatalytic degradation of water pollutants using bio-green synthesis of zinc oxide nanoparticles (ZnO NPs). *J. Environ. Chem. Eng.*, **vol. 9**, no. 4, p. 105772.
[25] Lê Phước Thảo Nguyên, Võ Viết Đại, Trần Thị Hằng, Nguyễn Trần Nguyên, (2019). Green chemistry towards the synthesis of some 2-pyrrolidinone derivative. *Journal of Analytical Sciences*, Vietnam analytical sciences society, **Vol 24**, No 1/2019, p 202-205.
[26] M. Shabaani, S. Rahaiee, M. Zare, and S. M. Jafari, (2020). Green synthesis of ZnO nanoparticles using loquat seed extract; Biological functions and photocatalytic degradation properties. *Lwt*, **vol. 134**, no. April, p. 110133.
[27] Z. Li, J. Dai, C. Cheng, Z. Suo, and W. Qing, (2020). Synthesis and magnetic properties of chromium doped cobalt ferrite nanotubes. *Mater. Res. Express*, **vol. 7**, no. 8, p. 6102.
[28] D. Gheidari, M. Mehrdad, S. Maleki, and S. Hosseini, (2020). Synthesis and potent antimicrobial activity of $CoFe_2O_4$ nanoparticles under visible light. *Heliyon*, **vol. 6**, no. 10, p. e05058.
[29] G. Sharmila, M. Thirumarimurugan, and C. Muthukumaran, (2019). Green synthesis of ZnO nanoparticles using Tecoma castanifolia leaf extract: Characterization and evaluation of its antioxidant, bactericidal and anticancer activities. *Microchem. J.*, **vol. 145**, pp. 578–587.